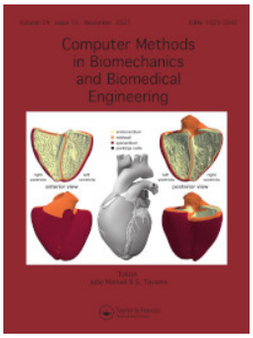

Taylor & Francis
Taylor & Francis Group

Computer Methods in Biomechanics and Biomedical Engineering

ISSN: (Print) (Online) Journal homepage: https://www.tandfonline.com/loi/gcmb20

Combined numerical and experimental approach to determine numerical model of abdominal scaffold

Agnieszka Tomaszewska & Daniil Reznikov

To cite this article: Agnieszka Tomaszewska & Daniil Reznikov (2021): Combined numerical and experimental approach to determine numerical model of abdominal scaffold, Computer Methods in Biomechanics and Biomedical Engineering, DOI: 10.1080/10255842.2021.2005788

To link to this article: https://doi.org/10.1080/10255842.2021.2005788

Published online: 28 Nov 2021.

COMPUTER METHODS IN BIOMECHANICS AND BIOMEDICAL ENGINEERING
https://doi.org/10.1080/10255842.2021.2005788

Combined numerical and experimental approach to determine numerical model of abdominal scaffold

Agnieszka Tomaszewska and Daniil Reznikov

Department of Structural Mechanics, Faculty of Civil and Environmental Engineering, Gdańsk University of Technology, Gdańsk, Poland

ABSTRACT

A proper junction of the prosthesis and the abdominal wall is important in successful hernia repair. The number of tacks should be balanced to assure appropriate mesh fixation and not to induce post-operative pain. Numerical simulations help to find this balance. The study is aimed at creating a proper numerical model of a knitted surgical mesh subjected to boundary conditions and load occurring in the abdominal cavity. Continuous, anisotropic constitutive relation is considered to reflect the mesh behaviour. Different sets of material law parameters are determined on the basis of different bi-axial tests setups. Force- and displacement-controlled tests with different ratios are considered. Consequently, some numerical model variants are obtained featuring various reaction distributions in the scaffold fixation points. The proper variant is selected based on comparison of the position of maximal reaction force in the numerical model and in the reference physical model of operated hernia. Force-driven tests have shown anisotropic mesh behaviour, while equibiaxial displacement-driven test has demonstrated reduced anisotropic response. Within seven scenarios of constitutive parameters identification (based on single or combined experimental data), the equibiaxial force-controlled test appeared to produce the most relevant model to follow the prosthesis behaviour under pressure. The position of maximal reaction force in such model is similar to obtained in the physical hernia model. The equibiaxial force-driven test provides most suitable data for Gasser-Ogden-Holzapfel constitutive model identification of a considered surgical mesh to be used to model the mesh under pressure.

ARTICLE HISTORY
Received 4 January 2021
Accepted 9 November 2021

KEYWORDS
Knitted prosthesis; hernia; bi-axial test; FE model of prosthesis; constitutive model identification

1. Introduction

Different solutions for ventral hernia management are discussed in the literature with the aim to find best ones in various medical cases (Baylón et al. 2017; Bittner et al. 2019). In the surgical intervention the hernia orifice is sewed or repaired with the use of mesh, which rebuilds abdominal wall in the orifice. The abdominal wall-implant system is therefore created. Mathematical modelling of the system helps to determine best medical solutions (Szymczak et al. 2017; Todros et al. 2017; He et al. 2020) and in a consequence to reduce hernia recurrence rate, which up to day is still very high, up to 25% in incisional hernia cases (Hoffmann et al. 2021). However, reliable data concerning geometry, boundary conditions, loading and constitutive model of the materials are required as an input for the numerical analysis.

This paper addresses constitutive modelling of surgical mesh, which is a complex, knitted structure. Different approaches to such material modelling are reported in the literature. Röhrnbauer et al. discussed three scales of the prosthesis modelling: global and yarn scales, and mesoscale (Röhrnbauer et al. 2014). The authors proposed mesoscale model of a mesh, however they showed an example for a single unit cell. Pierrat et al. presented a preliminary study to consider the three scales of surgical mesh modelling (Pierrat et al. 2020). The authors recommend yarn scale to apprehend local failure modes in these structures. Hernandez-Gascon et al. compared the outcomes of the global and the yarn scales and recommended the global continuum model, which provided a greater computational efficiency and a higher convenience in application into complex numerical models (Hernández-Gascón et al. 2014). Continuum model is sufficient to study global response of knitted structure. In reference to that an

CONTACT Agnieszka Tomaszewska atomas@pg.edu.pl

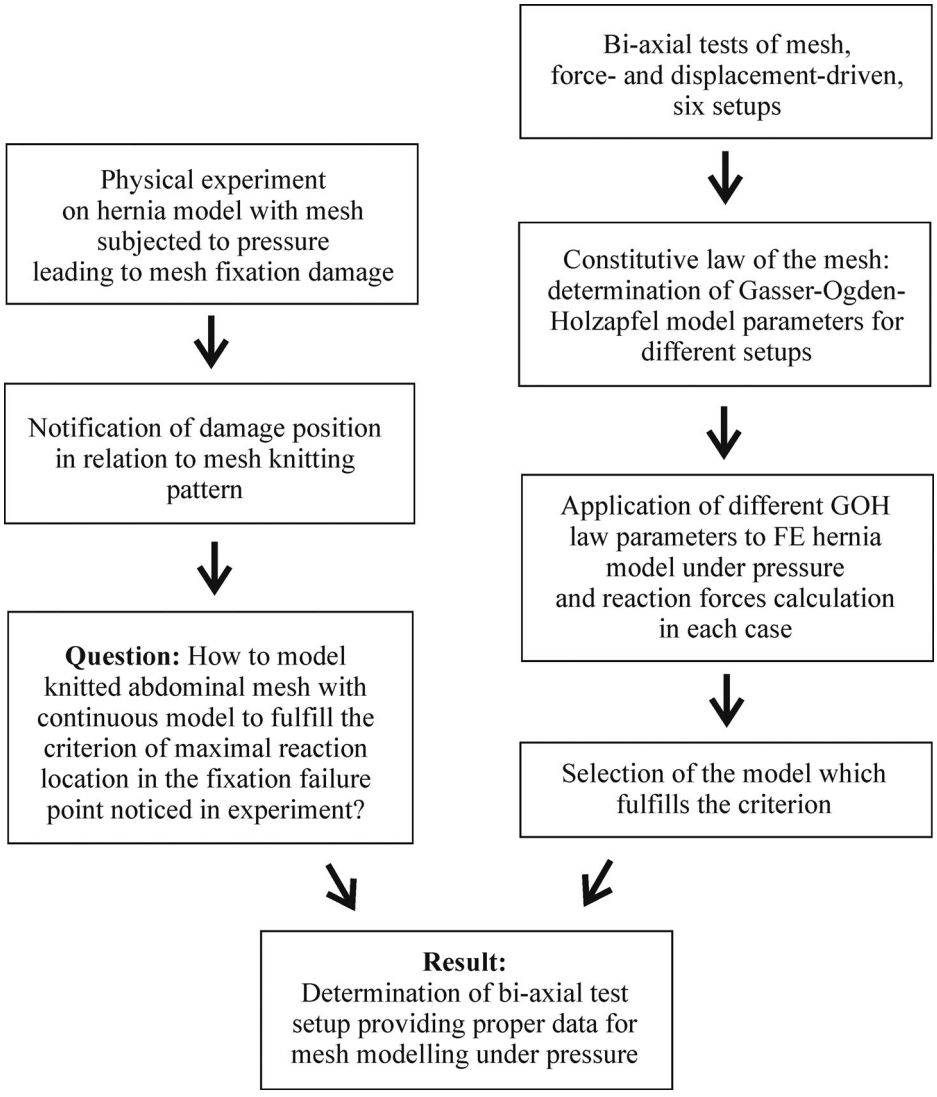

Figure 1. Flow chart of methodology developed in the paper.

issue concerning continuum model of a surgical mesh is considered in this paper.

The prostheses reveal anisotropic properties in most cases, two approaches are present in the literature so far to cover their homogeneous constitutive models. The first is the dense net material model, in which two axes of the material are distinguished, inclined by the deformation-related angle (Branicki and Kłosowski 1983; Lubowiecka 2015a). The second considers an anisotropic hyperelastic material model defined by strain energy function (Hernández-Gascón et al. 2014; Horbach and Staat 2018).

Mechanical tests are necessary to trace material behaviour under loading and to determine the constitutive relation. The authors in Deeken and Lake (2017) present the advances on the tests performed on abdominal meshes. Several groups employ uniaxial tension tests to identify strength and stiffness of the material (Saberski et al. 2011; Todros et al. 2018; Rynkevic et al. 2019) or to identify anisotropic material constitutive law (Hernández-Gascón et al. 2011). The issues of material viscoelasticity (Li et al. 2014) and material strain-hardening due to cyclic loading (Velayudhan et al. 2009; Tomaszewska 2016) are also discussed. Biaxial tests reproduce the physiological loading of the prosthesis better than uni-axial. These tests were performed to determine anisotropy ratio, peak tension and strain values of 20 sorts of meshes (Est et al. 2017). The authors have made displacement-driven equibiaxial setup, where the samples were equally stretched in two perpendicular axes and directional strip tests (stretching along one axis while the other axis is held fixed). Other researchers have made force-driven tests in equibiaxial setup, or with the force ratio 1:0.5 (Cordero et al. 2016) to determine anisotropy ratio and stiffness of six meshes. Also the parameters of anisotropic hyperelastic material

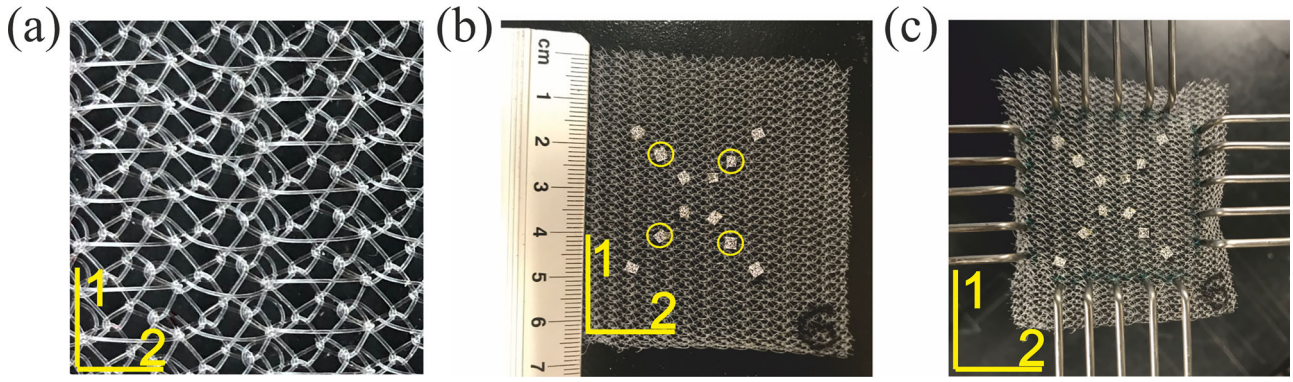

Figure 2. (a) Knitting pattern of DynaMesh-IPOM, (b) Sample prepared for the test, (c) Sample mounted in rakes.

model are identified, however, the authors do not show its application in a numerical model.

Planar soft tissues are similarly tested and modelled, some conclusions from these studies may be transferred to abdominal prostheses. The difference has been studied between stress-strain relations of a planar connective tissue in biaxial tests using clamp grips or suture grips (Waldman et al. 2002). The authors have found that the clamped specimen mounting increases the sample stiffness compared to suture mounting. However, suture mounting is difficult to replicate among a set of specimens. This is the origin of rake invention. The influence of varying conditions of biaxial test with the use of rakes on the parameters of soft tissue constitutive model has been studied in Fehervary et al. (2016). The authors compared the outcome of different loading protocols. The influence of the data selection for deformation gradient determination and of the stress definition on the quality of the parameter fitting results has been reported too. The authors recommended the application of rakes in biaxial testing, strain tensor definition based on markers tracking and stress definition related to a distance between the outer needles of the rakes.

Experiments of the field out of biomedical domain are also possible to consider. Van Craenenbroeck et al. investigated a case of polyester-PVC fabric. Here the parameters of constitutive model were shown to depend on the load profile applied in the bi-axial test (Van Craenenbroeck et al. 2019). The authors pose a question on how the uncertainty of the model parameters should be incorporated into the design process.

Thus, still unclear is how biaxial tests should be controlled to determine parameters of the constitutive model of a knitted mesh to reflect its performance properly. In reference to that the authors study here the impact of force- or displacement-control in a biaxial test on the identified anisotropic constitutive model parameters and on the outcome of finite element (FE) model of a surgical mesh with boundary conditions and loading reflecting the mesh location in the abdominal wall. The aim is to determine the setup bringing a comparable simulated response of the prosthesis to a pressure load to the experimentally observed behaviour. The reference physical hernia model built of a porcine tissue and synthetic prosthesis is described in Tomaszewska et al. (2019). In the course of an air impulse strike a single fixation point was damaged in that model – the highest reaction force occurred in this point. The numerical model (and the bi-axial test setup, which delivered data for constitutive model used in it), leading to an extreme reaction force at the same fixation point as in the experiment is considered relevant. The roadmap of the analysis is presented in Figure 1.

2. Materials and methods

2.1. The considered mesh

DynaMesh-IPOM (FEG Textiltechnik GmbH, Aachen, Germany) is a synthetic, knitted mesh, whose polypropylene filaments are interlinked with polyvinylidene fluoride threads. The knitting pattern is shown in Figure 2(a). In the previous study (Tomaszewska 2016), the material was subjected to uni-axial tensile tests. Tension was applied in the direction of the knitting pattern (‘1’ direction of the material) and in perpendicular direction (‘2’ direction). The tests showed the mesh higher strain limit in the direction ‘1’ than in the direction ‘2’ and a lower stress limit in the direction ‘1’ compared to the direction ‘2’. The mesh orthotropy ratio, defined as a ratio of elastic moduli in two considered directions, changes with the strain magnitude, starting from 4.7 while the strain is smaller than 0.3 and reaching 3.3 for the strains between 0.3 and 0.6 (direction ‘2’ is always stiffer).

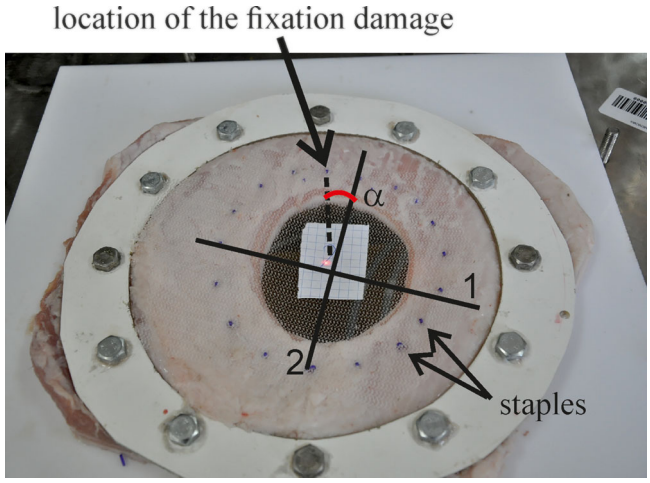

Figure 3. Physical hernia model showing fixation damaged by an impulse pressure load.

2.2. The reference experiments

The study refers to *ex vivo* experiments made on operated hernia models (physical models) built of DynaMesh-IPOM and a porcine abdominal wall with a 7 cm wide orifice (see Figure 3). The 'hernia' orifice was managed by the mesh mounted in the tissue by regularly spaced point sutures or staples. The diameter of the fixation circle was 13.5 cm. A 5 cm mesh-tissue overlap was preserved. The model was located in a pressure chamber (Tomaszewska et al. 2019) and pressure-loaded. To prevent air leakage through the porous mesh the whole model was covered by a thin loose foil not disturbing model displacements.

Two sorts of tests were performed to complete two tasks, the specification reads below.

2.2.1. Tests with dynamic loading (TD tests)

High pressure level, between 21 and 32 kPa, was applied in the tests to produce fixation failure, the position of the damaged junction was detected. Three models in an experiment were built, employing ETHICON SECURESTRAP Stapler (ETHICON, Inc., Somerville, NJ 08876, USA). The staples were spaced every 2 cm (2 models) or every 4 cm (1 model) but in the fixation ring they were shifted in different ways from the '2' axis of the mesh. The three models showed the damage of a single fixation point. This fixation was located at $\alpha = 15$, 20 or 32°, the average inclination is 22°, from the '2' direction of the mesh as marked in Figure 3. The α angle defines the axis of the greatest reaction force in the domain of all reactions in the mesh fixation points due to pressure loading.

2.2.2. Test with static loading (TS tests)

A single model was statically loaded by 7.75 kPa pressure to obtain data for the FE model validation. The prosthesis was fixed in the tissue by 19 trans-abdominal sutures spaced every 2 cm, this geometry was reflected in numerical model. The final pressure was reached within 4 s. The deflection of the model central point under this load was 31.5 mm.

2.3. Biaxial tests setup

2.3.1. Sample preparation and mounting in the machine

Nine square pieces (65 × 65 mm) of the mesh were prepared for the experiment (Figure 2(b)). They were cut out of a single prosthesis. Sides of the squares were cut along the knitting pattern of the implant and in a perpendicular direction. The samples were subjected to biaxial tensile tests in a Biax Zwick Roell machine with the 500 N load cells. The samples were mounted in the machine using rakes (Figure 2(c)) which needles were carefully placed in the prosthesis pores. As the pores are aligned to the mesh knitting pattern direction, such mounting preserves similar initial condition in all samples. Moreover, it resembles real fixation in the abdominal wall, where the mesh is fixed in a set of points.

2.3.2. Loading protocols

Two loading protocols were included in the tests. The first considers force-driven experiments, the second includes displacement-driven tests. In the force-driven test course four force ratios were regarded in the following relation to the axes 1–2 of the mesh: 1:1.5 (tests code F_1:1.5), 1.5:1 (F_1.5:1), 1.2:1 (F_1.2:1), 1:1 (F_1:1). The speed of force action in the tests was 0.125 N/s in one direction (basic speed), in the second direction the speed was higher to obtain the designed force ratios. In the displacement-driven protocol two

displacements ratios were applied to the axes 1–2 of the mesh: 1.5:1 (D_1.5:1) and 1:1 (D_1:1). The opposite to D_1.5:1 case displacements ratio, i. e. 1:1.5, was not considered as it is not physiologically recommended in the abdominal wall. It is known that human abdominal wall stretches more in the cranio-caudal axis than in the transverse direction, so the mesh should be accordingly oriented in the wall, i.e., more elastic axis of the mesh should be placed along the spine to minimize forces in the mesh fixation points (Szymczak et al. 2017). The basic displacement ratio in both tests was 1 mm/min (the lower one). The force limit in the force-driven tests was set to 20 N and in the displacements-driven tests it was assumed 30 N. Due to a limited number of samples a selected test, D_1:1 was repeated three times to check out repetitive character of the results. While it was confirmed, the following tests were conducted once.

2.3.3. Strain measurements

The strain tensor in the sample central point was determined with the use of four markers and assuming homogeneous stress field within the region limited by the markers, as proposed in Sacks (2000). The Q-400 DIC Multicamera system (DANTEC DYNAMICS GmbH, Ulm, Germany) equipped with two cameras DANTEC VCXU-23M of 2.3 MPx resolution (1920 × 1200 px) and Istra 4D V4.4.7.908 software was employed to track the marker displacements. Square markers of 2 mm side length were applied. The markers were mounted to the sample using elastic butapren glue to reduce the markers-sample coupling effect, addressed in Todros et al. (2019). To avoid the non-homogeneous stress field due to the Saint Venant's principle, the position of markers was determined in a preliminary study considering three distances between the markers: 1 cm (M1 set), 2 cm (M2 set) and 3 cm (M3 set), see Figure 3(a). The strain tensors measured by the M1 and M2 sets were identical, so in further tests the M2 set was used (the M2 set is marked by yellow circles in Figure 3(a)).

The samples were tested at room temperature, in dry conditions. The mesh hydration does not affect the results of the mechanical tests obtained for the material considered here, as discussed in Tomaszewska (2016).

2.4. Constitutive model and the parameters identification based on biaxial test

As the considered prosthesis reveals anisotropic hyperelastic properties (Tomaszewska 2016), the Gasser–Ogden–Holzapfel (GOH) model is selected to reflect mechanical behaviour of the mesh (Gasser et al. 2006). The model covers stress-strain relations in anisotropic, fiber-reinforced materials. Two preferential directions of the material are determined in the parameters identification process. Similar constitutive model of knitted abdominal meshes is selected in study described in Hernández-Gascón et al. (2013). The strain energy density function (SEDF) of a model with two families of fibers is stated by Equation (1). The SEDF consists of two components. The first term captures isotropic material behaviour (the material matrix contribution), and the second reflects anisotropic material behaviour (the contribution of fibers embedded in the matrix). Although the considered prosthesis shows a different physical structure this model, combining isotropic and anisotropic material response is relevant here. The parameter responsible for the fiber orientation points at anisotropy axes of the mesh.

$$\psi = C_{10}(I_1 - 3) + \sum_{i=4,6} \frac{k_1}{2k_2}\left(e^{k_2(\kappa I_1 + (1-3\kappa)I_i - 1)^2} - 1\right) \tag{1}$$

This equation involves the following: C_{10} and k_1, which are the stress-like parameters, k_2 is the dimensionless parameter and κ which covers dispersion of the fibers. The term I_1 is the first invariant of the Cauchy-Green strain tensor $\mathbf{C} = \mathbf{F}^T\mathbf{F}$, where $\mathbf{F}$ denotes deformation gradient.

$$I_1 = tr(\mathbf{C}) \tag{2}$$

The terms I_4 and I_6 are two pseudo-invariants of $\mathbf{C}$, they cover the behaviour of the fiber families

$$I_4 = \mathbf{a}_0 \cdot \mathbf{C}\mathbf{a}_0\,, \quad I_6 = \mathbf{g}_0 \cdot \mathbf{C}\mathbf{g}_0, \tag{3}$$

$$\mathbf{a}_0 = \begin{bmatrix}\cos(\gamma) & \sin(\gamma) & 0\end{bmatrix}^T,$$

$$\mathbf{g}_0 = \begin{bmatrix}\cos(\gamma) & -\sin(\gamma) & 0\end{bmatrix}^T, \tag{4}$$

where γ, in this study, denotes the angle between the '2' direction of the material and the fiber families. The vectors $\mathbf{a_0}$ and $\mathbf{g_0}$ are the unit vectors which determine the fiber orientation in the undeformed configuration (Holzapfel 2000). The second Piola-Kirchhoff stress tensor involves derivatives of the SEDF with respect to the measures of deformation. In the case of incompressible material the following formula is valid:

$$\mathbf{P}^{II}_{mod} = -p\mathbf{C}^{-1} + 2\frac{\partial\psi(\mathbf{C})}{\partial\mathbf{C}}, \tag{5}$$

where p is the Lagrangian multiplier, to be obtained from the boundary conditions.

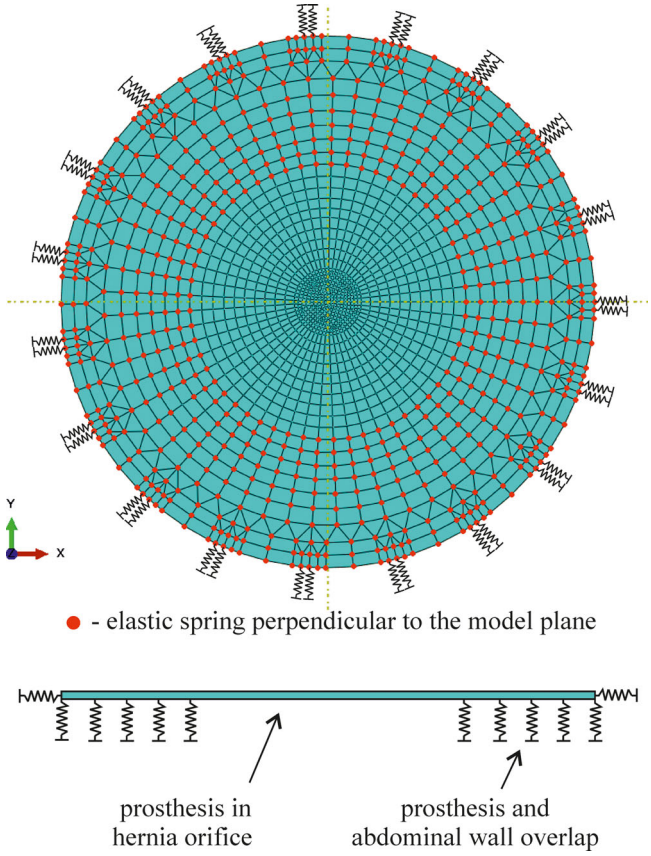

Figure 4. View of the numerical model.

The Cauchy stress tensor is composed with the assistance of deformation gradient:

$$\boldsymbol{\sigma}_{mod} = \mathbf{F}\mathbf{P}^{II}_{mod}\mathbf{F}^{T}. \tag{6}$$

Material deformation in planar biaxial test is covered by the relations $x_1 = \lambda_1 X_1 + \gamma_1 X_2$; $x_2 = \lambda_2 X_2 + \gamma_2 X_1$; $x_3 = \lambda_3 X_3$, where X and x denote the location of markers in the reference and deformed states, respectively, λ are the stretches and γ are the shear measures (Sacks 2000). The material is considered incompressible, therefore λ_3 yields from the condition $\det\mathbf{F} = 1$. The displacement field $\mathbf{u} = \mathbf{x} - \mathbf{X}$ can be obtained using the finite element shape function (Sacks 2000)

$$\mathbf{u}(r,s) = \sum_{n=1}^{m} f_n(r,s)\mathbf{u}_n, \tag{7}$$

where f_n is the shape function of markers n, m denotes the total number of markers, and r, s are isoparametric coordinates. Hence, the deformation gradient is given by:

$$\mathbf{F} = \mathbf{I} + \frac{\partial \mathbf{u}}{\partial \mathbf{X}}, \tag{8}$$

where $\mathbf{I}$ is the identity matrix.

The parameters of the model are identified on the basis of stress-strain relation investigated in biaxial tensile tests of the material. An optimization procedure is employed to identify parameters of a theoretical stress-strain relation i.e., the constitutive model. In the bi-axial case the objective function takes the following form

$$\chi^2 = \sum_{s}\sum_{j=1}^{k}\left[\left(\sigma_{exp,11} - \sigma_{mod,11}\right)_j^2 + \left(\sigma_{exp,22} - \sigma_{mod,22}\right)_j^2\right], \tag{9}$$

here $\sigma_{exp,11}$, $\sigma_{exp,22}$ are the Cauchy stress tensor terms in tension directions (1 and 2, respectively) determined experimentally, $\sigma_{mod,11}$, $\sigma_{mod,22}$ are corresponding stresses determined by the constitutive model. The parameter k denotes the number of the stress data points measured for samples s. Within such definition of the optimization process a single experiment or a combination of tests can be considered. Such approach is addressed e.g. in Fehervary et al. (2018). In the study the objective function is minimized with respect to five parameters of the constitutive model with the use of trust-region-reflective variant of the least square method applied in the *lsqnonlin* function in Matlab R2016b (The

MathWorks, Natick, MA, USA). The optimization quality measure is the normalized mean square root error $\varepsilon = \frac{\sqrt{\frac{\chi^2}{ks-q}}}{\mu}$, proposed in Hernández-Gascón et al. (2011), where q is a number of parameters of the objective function, $ks = \sum_s 2k$ is a number of all stress data introduced in χ^2, the difference ks-q is the number of degrees of freedom. Finally, $\mu = \frac{1}{ks}\sum_{j=1}^{ks}\sigma_j$ denotes the mean stress of an entirety of data.

The experimental (nominal) stress is defined by the first Piola-Kirchhoff stress as a ratio of the traction force t_i in the i-th direction and the undeformed section surface perpendicular to the i-th direction $A_{i,0}$

$$P^I_{exp,ii} = \frac{t_i}{A_{i,0}}, \; i = 1,2,3. \tag{10}$$

In the case of the incompressible materials the Cauchy stress $\boldsymbol{\sigma}_{exp}$ is related to the first Piola-Kirchhoff stress by the deformation gradient $\mathbf{F}$ (Holzapfel 2000) as follows:

$$\boldsymbol{\sigma}_{exp} = \mathbf{P}^I_{exp}\mathbf{F}^T. \tag{11}$$

Definition of $A_{i,0}$ is not evident in the case of discontinuous material and discontinuous fixation, these are cases considered in the study. The three following definitions of $\boldsymbol{\sigma}_{exp}$ may be considered: the length covered by the rakes; the rake width and the specimen width. The length covered by the rakes leads to a high agreement between the experimental and the model stresses according to Fehervary et al. (2016). Thus, the study also accepts this issue. The material thickness is assumed 1 mm in experimental and numerical stress assessment.

2.5. Numerical simulation

2.5.1. Numerical model definition

The model was built in SIMULIA Abaqus FEA 2019. The considered prosthesis was modelled as a circular membrane of a 13.5 cm diameter, responding to the fixation circle in the physical model. The M3D4 and M3D3 finite elements with four nodes and three nodes, respectively, and three translational degrees of freedom in each node were employed. In the physical model, the mesh was fixed in the abdominal wall acting as elastic medium. Thus, following the concept introduced in Lubowiecka (2015b), the mesh FE model was supported by elastic springs. Springs perpendicular to the model plane were situated in the region of the mesh and tissue overlap. The springs in the model plane were assumed in the location of 19 mesh fixation points in the physical model. They were spaced by every 18.9 degrees and oriented in the model radial direction. Two adjacent nodes were supported this way in each support. The stiffness of the springs was determined in the model validation process. The model overview is presented in Figure 4. The GOH constitutive model, available in ABAQUS package was applied to the membrane. The angle γ of fiber orientation is measured with respect to the global x axis of the model, in fact, the '2' direction of the prosthesis. The set of models created was diverse due to constitutive model parameters based on subsequent bi-axial tests with different set-ups.

2.5.2. Analysis

The model was loaded with a 7.75 kPa pressure within 4 s. Geometrical and material nonlinearities trigger an instability problem in the static analysis of the membranes. Hence, dynamic implicit analysis was performed, with the Hilber-Hughes-Taylor time integration and with artificial damping associated with this method (Abaqus documentation 2017). The model convergence was checked comparing the model stresses and deflections in the case D_1:1_1 in two density variants of finite elements. The first model incorporated 8265 elements, the other one employed 2406. Maximum deflections in both models showed a relative 1% scatter and the maximal difference between principal stresses in the nodes adjacent to the mesh fixation points was 5%. The mesh built of 2406 elements was chosen for further simulations. The selected mesh is presented in Figure 4.

Each of the considered models was validated to the deflection of the mesh central point, as measured in the experiment. Stiffness of the supporting springs acted as a validated parameter, determined in two steps. First of all, stiffness in every considered model was validated to obtain the desired deflection. Next, stiffness was averaged over the set of models. An identical, averaged spring stiffness was finally set in all models considered. That allowed to objectively compare the results obtained in the cases of different models. Stiffness of the springs perpendicular to the mesh plane has bound to form on elastic support of 0.011 MPa stiffness. Stiffness of springs in the radial direction of the mesh was 0.75 MPa.

Finally, reaction forces in the model plane were assessed in each model subjected to 7.75 kPa load. The collected values were further compared to determine the model to make the maximum reaction force collinear with the axis oriented by the angle of $\alpha = 22^\circ$ to the '2' axis of the prosthesis. The model selected this way points at constitutive model

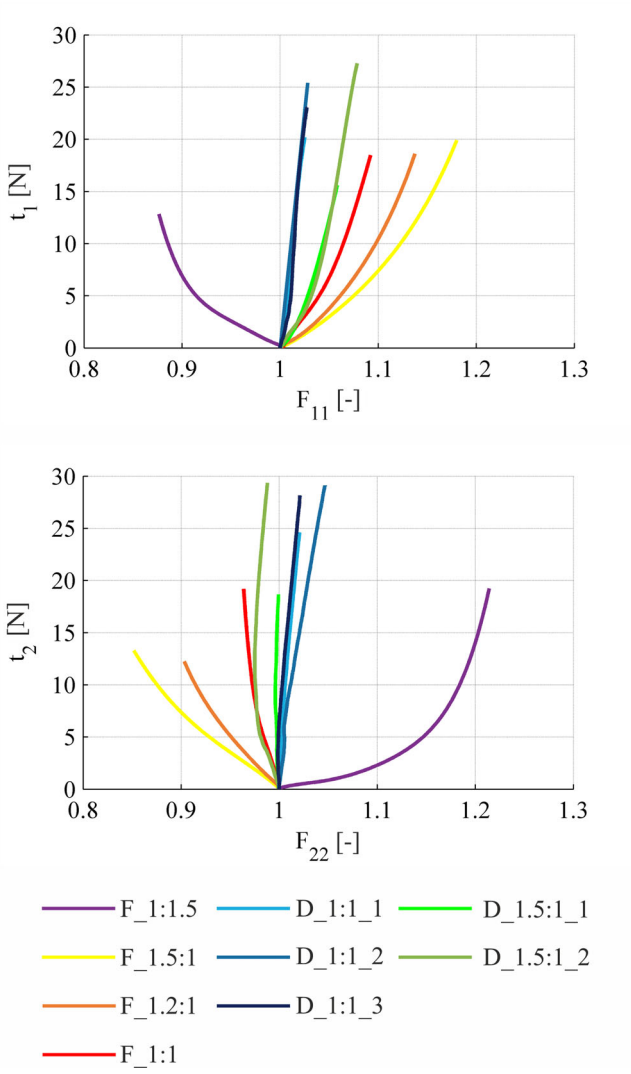

Figure 5. Traction force as a function of deformation obtained in six experimental cases.

parameters and at the biaxial test setup, which lead to a physically confirmed result.

3. Results

3.1. Biaxial tests of the mesh

Traction forces at the rakes and the in-plane displacements of the markers were measured in the test course. They helped to determine the Cauchy stress tensor and Cauchy-Green strain tensor, as noted in Sect. 2. The diagonal elements of the tensors were selected to draw their interrelation in the directions of the applied load. All the obtained curves are presented in Figure 5. The repetitive character of the results is confirmed in the test D_1:1. The response measured in the D_1.5:1 case is qualitatively different than the ones observed in other cases. Reduction of the deformation gradient in the '2' direction is observed at the test start, next, it grows up starting from the 8 N force. Such a curve is not covered by the GOH model with a satisfactory tolerance. The test has been repeated with a doubled speed to yield a similar qualitative result. Thus, the D_1.5:1 case is excluded from further analysis.

3.2. Constitutive model parameters

The optimization task (9) showed a single solution in each case, within the accepted boundary limits. The parameters of the GOH constitutive model obtained for various experimental cases, single and combined, are presented in Table 1 along with the ε error. Two combined cases have been considered as follows: F_1.5:1 + F_1:1.5 and F_1.5:1 + F_1:1 + F_1:1.5. They are symmetrical as regards load applied to the samples. The curve fitting results of single cases are plotted in Figure 6, with regard to the experimental curves.

Table 1. Parameters of GOH constitutive model obtained for different experimental cases and the FE models deflections.

		Parameter							
		C_{10} (N/mm^2)	k_1 (N/mm^2)	k_2 (-)	γ (°)	κ (-)		Deflection in the mesh	
Boundary	Lower	0.05	0	0	0	0		central	Max
limits	Upper	10	1000	1000	90	1/3	MSRE (-)	point (mm)	reaction (N)
Single	F_1:1.5	0.05	0.199	136	45	0	0.0488	35.1	1.37
experimental	F_1.5:1	0.05	1.83	172	46	0	0.0691	32.2	2.14
cases	F_1.2:1	0.05	1.60	158	46	0	0.0455	32.4	2.08
	F_1:1	0.123	53.0	2.2e-14	37	0.227	0.0383	30.1	2.38
	D_1:1	1.20	5.09	2.2e-14	40	0	0.0403	28.2	1.77
Combined	F_1:1.5+	0.05	0.953	156	48	0.039	0.234	33.4	2.01
cases	F_1.5:1								
	F_1:1.5+ F_1.5:1+ F_1:1	0.05	1.89	33	48	0	0.418	32.5	1.72

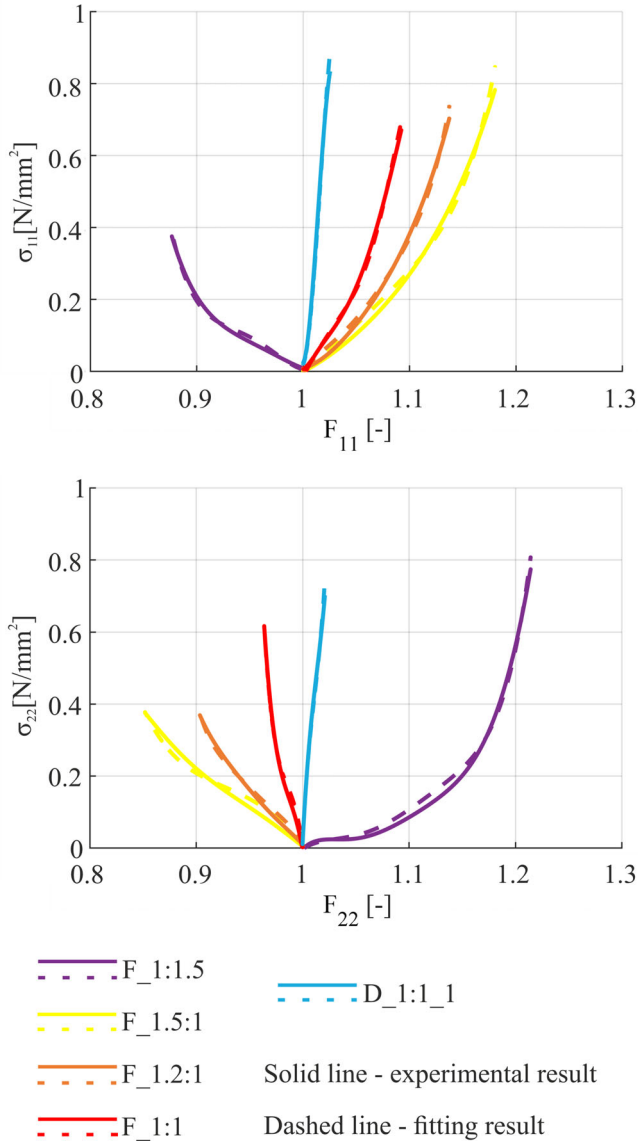

Figure 6. Stress as a function of deformation. Theoretical and experimental relations for the considered single cases.

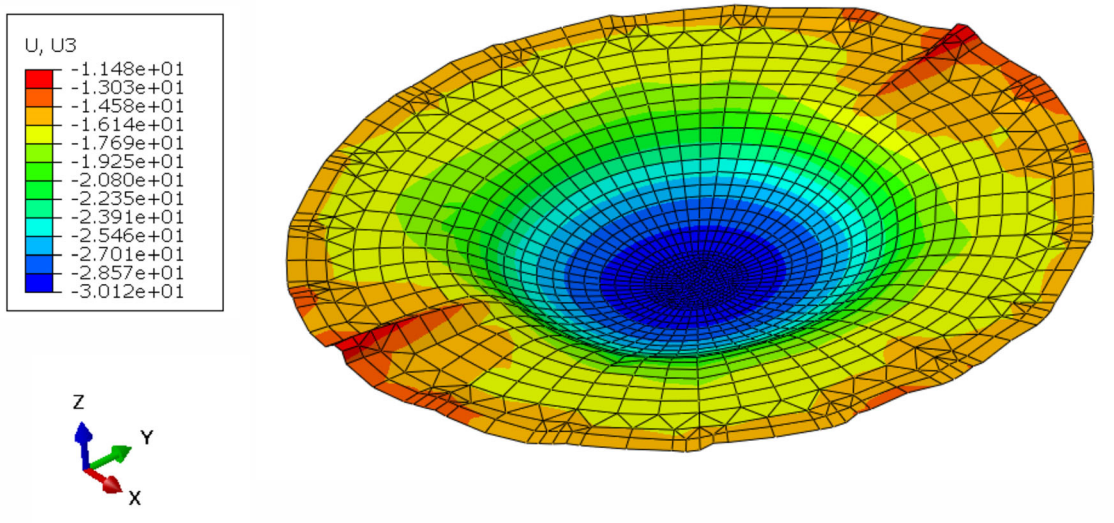

Figure 7. Deformation of the F_1:1 model under pressure load.

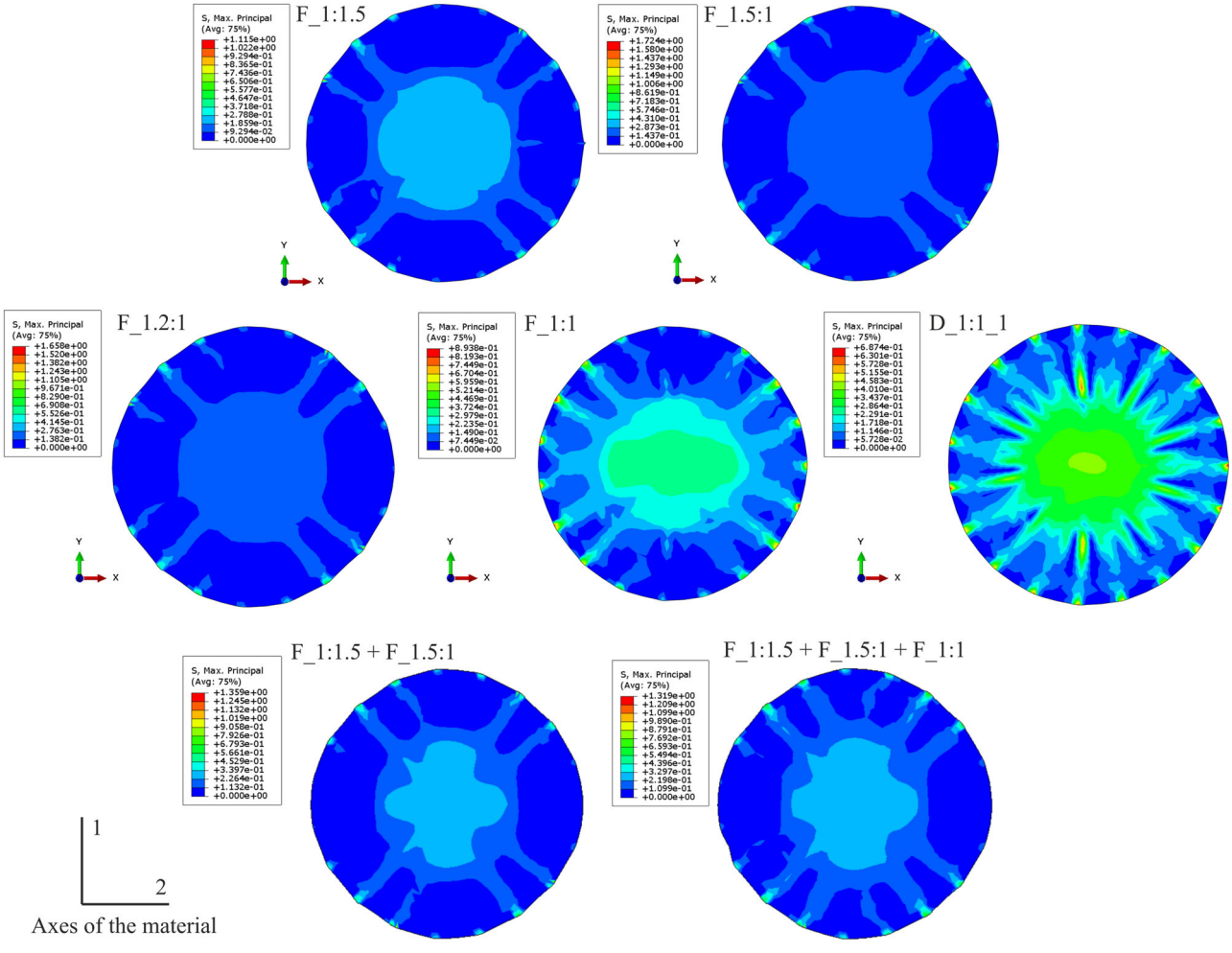

Figure 8. Principal stress in the seven considered cases.

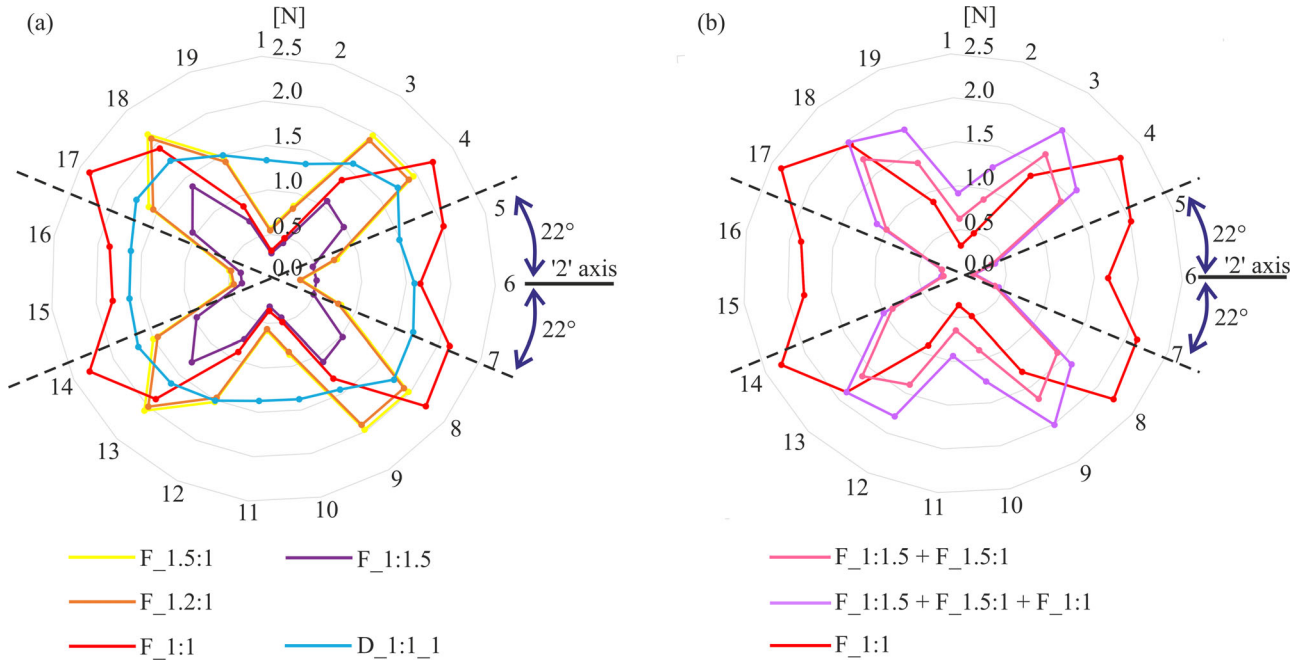

Figure 9. (a) Reaction forces calculated for each single case, (b) Reaction forces calculated for two combined cases and in the F_1:1 case.

3.3. Numerical simulations

Deformation of the F_1:1 model under pressure is presented in Figure 7. Other models behave similarly. Deflection of the mesh central point is given in Table 1. The maps of the principal stresses in seven considered cases are presented in Figure 8. The reaction forces in the mesh fixation points computed in each case are shown in Figure 9. The material axis '2' is marked along with the axis of the fixation failure determined in the TD reference experiments (see Figure 3).

4. Discussion

4.1. Influence of the biaxial test setup on constitutive model parameters and FE model results

Traction force vs deformation gradient relations (Figure 5) obtained in the study show various responses of the samples to the applied actions. In the displacement-controlled test variant D_1:1 the impact of mesh anisotropy is reduced. It raises up the C_{10} parameter of the constitutive law (1). This parameter is at least 10 times smaller with reference to other test results (see Table 1). Thus, nearly axisymmetric principal stresses and reaction forces are obtained on the basis of this test (Figures 8 and 9(a)). Such outcome cannot be assumed physically true, while the TD tests detect the damaged fixation point situated in a constant region of the mesh (the mean inclination 22°, with regard to the '2' axis of the mesh), i.e., the highest reaction force appears there when the mesh is subjected to pressure. A conclusion arises that equibiaxial displacement-controlled test does not provide relevant identification data of the considered constitutive law to be employed in the FE model of the prosthesis under pressure.

The relations presented in Figure 5 considerably differ between force-controlled tests. In the previous study on mechanical properties of DynaMesh-IPOM (Tomaszewska 2016) a higher stiffness of the material along '2' axis has been stated with regard to '1' axis. This result justifies the mesh extension in the '1' direction throughout the F_1:1 test (see Figure 5). Extension in this direction occurs also while a greater force acts along '1' axis (tests F_1.2:1 and F_1.5:1), shortening happens when a greater load is applied along '2' axis, in the latter case extension occurs in the '2' direction of the sample. These diverse performance modes produce various parameters of the constitutive equation (Equation (1)) however only equibiaxal tension test brings results considerably different from the results of other three force-controlled tests. The parameters based on F_1.2:1, F_1.5:1 and F_1:1.5 cases are similar. The orientation of fibers γ based on these three tests is 45° and 46°, the dispersion of fibers κ is nearly zero, the C_{10} parameter

equals 0.05. Based on the F_1:1 test the impact of the isotropic part is higher, as $C_{10} = 0.123$ and $\kappa = 0.227$, and $\gamma = 37^\circ$ is the closest to the axis of the damage observed in the TD tests. The γ angle suggests that the F_1:1 test is the most suitable to identify constitutive law in the studied case, confirmed in the FE prosthesis model. Regarding the results of TD tests each model is investigated to detect maximum reaction force in the supports no. 5, 7, 14, 17, the closest to the axes oriented by ±22° to the '2' direction of the material (marked in Figures 3 and 9). It is obtained in the F_1:1 case, noticed in Figure 9. The principal stress distribution in this model yields the extreme values aligned in the '2' axis of the material (Figure 8). It means that the equibiaxial force-controlled test produces the most relevant model to follow the prosthesis behaviour under pressure.

Other three force-controlled tests and the two combined cases provide qualitatively similar results, which differ from the results based on F_1:1 test. The maximum reaction forces in FE models based on the presented five cases always occurs at supports no. 3, 9, 13, 18, shifted from the material axis '2' by ±46° or ±55°. The principal stresses increase also along these angles, as shown in Figure 8. The parameters of the constitutive law are similar between these five cases (see Table 1).

4.2. Value of the maximum reaction force

Value of the maximum reaction force is another important issue in surgical practice as prosthesis fixation strength is bound to resist the reaction forces. Different values of reactions emerge in the cases considered in the paper, as noticed in Table 1. These values may also depend on the constitutive law selected for the prosthesis modelling. The GOH model discussed in the paper sufficiently covers mechanical behaviour of DynaMesh, as the maximum reaction force is observed in the location of fixation damage noticed in the reference (TD) experiment. However, the TS experiment modelled in this study, was previously modelled by another constitutive law for the implant, i.e., the dense net material (DNM) model (Tomaszewska et al. 2019). The maximum principal stress distribution presented in that paper shows locations of maximum reaction forces also at the points surrounding material axis '2'. Thus, qualitative results of the FE models with GOH and DNM constitutive laws are similar. In a quantitative meaning they differ since maximum reaction force in the model with DNM is 0.87 N while the model with GOH shows it 2.38 N in the F_1:1 case, this value reduces in other cases. The knowledge is insufficient with regard to reaction forces in the mesh fixation *in vivo*. The limit values are known with respect to selected staples, however they have been determined *ex vivo*, in pulling test. The values measured using human body specimens and Symbotex composite mesh belong to the interval 13.6 N and 21.5 N in the group of ReliaTack, AbsorbaTack, ProTack, SorbaFix, SecureStrap (Chan et al. 2018). Both maximum reactions, obtained in DNM and GOH models, are lower that the limit values of the mentioned staples. Still more experimental works are required to determine the reactions and their distribution in the mesh fixation points in laparoscopic ventral hernia repair (LVHR).

4.3. Remarks on possibilities of in vivo observations of implanted mesh behaviour

The FE model applied in the study is limited due to its boundary conditions reflecting the abdominal wall. The *in vivo* research on a living abdominal wall with the implanted mesh are the prospective studies, which may help to determine the boundary conditions more specifically. Some recent works discuss mechanical behaviour of implanted mesh *in vivo*. The Roentgen pictures of patients after LVHR were analyzed in Lubowiecka et al. (2020), in these cases extension of the implanted mesh due to body side bending was determined. Radio-opaque beads on the implanted mesh were applied to visualize the 3D mesh stretch patterns on fluoroscopic images (Kahan et al. 2017). Finally, magnetic-visible intraperitoneal onlay mesh was employed to study the mesh demarcations and area (Köhler et al. 2015).

5. Concluding remarks

The study addresses the relation of the simulated behaviour of a surgical prosthesis and the control of the bi-axial test, aimed at collecting data for constitutive prosthesis model. The equibiaxial force-driven test provides most suitable data for Gasser-Ogden-Holzapfel constitutive model identification of a considered prosthesis. That is stated comparing the numerical model of the prosthesis response to the pressure load with the outcome of the physical model at the same load. It means that the equibiaxial force-controlled test produces the most relevant model to follow the prosthesis behaviour under pressure. Displacement-driven tests provided numerical model

results much different from the expected ones, based on the experiment. The force-driven biaxial tests with unequal force ratio provided intermediate outcome.

The study enhances the knowledge concerning force estimation in the mesh fixation points in LVHR using numerical model. However, true values of reaction forces have not been precisely determined yet. Further studies are required on FE modelling of knitted hernia prostheses.

The selected constitutive model is suitable to reflect the considered mesh behaviour, as the agreement between numerical and physical models has been shown. The model parameters obtained in the recommended setup point at the material anisotropy as $\kappa = 0.23$. A new observation concerning the prosthesis reveals that the anisotropy axes do not coincide with its knitting pattern, instead, the axes are oriented by the angle $\gamma \approx 37^\circ$ to the '2' direction of the material. Hence, the uni-axial tests, provided in some studies to collect basic information on the mesh mechanical properties should be conducted also in the mesh preferential directions in addition to the tests in the directions of its knitting pattern.

Disclosure statement

No potential conflict of interest was reported by the authors.

Funding

This work has been supported by the National Science Centre (Poland) (grant no. UMO-2017/27/B/ST8/02518). Calculations have been partially carried out at the Academic Computer Centre in Gdansk.

ORCID

Agnieszka Tomaszewska http://orcid.org/0000-0001-5680-7979
Daniil Reznikov http://orcid.org/0000-0001-5577-2057

References

Abaqus documentation. 2017. [accessed 2021 Jul 27]. https://abaqus-docs.mit.edu/2017/English/SIMACAEANLRefMap/simaanl-c-dynamic.htm.

Baylón K, Rodríguez-Camarillo P, Elías-Zúñiga A, Díaz-Elizondo JA, Gilkerson R, Lozano K. 2017. Past, present and future of surgical meshes: a review. Membranes (Basel). 7(3):47–53.

Bittner R, Bain K, Bansal VK, Berrevoet F, Bingener-Casey J, Chen D, Chen J, Chowbey P, Dietz UA, de Beaux A, et al. 2019. Update of guidelines for laparoscopic treatment of ventral and incisional abdominal wall hernias (International Endohernia Society (IEHS))—part A. Surg Endosc. 33(10):3069–3139.

Branicki C, Kłosowski P. 1983. Statical analysis of hanging textile membranes in nonlinear approach. Arch Civ Eng. XXIX:189–219.

Chan YW, Sow Z, Lukic D, Monschein M, Calek E, Pretterklieber M, Hollinsky C. 2018. Comparison of mesh fixation devices for laparoscopic ventral hernia repair: an experimental study on human anatomic specimens. Surg Endosc. 32(7):3158–3163. doi:10.1007/s00464-018-6031-5.

Cordero A, Hernández-Gascón B, Pascual G, Bellón JM, Calvo B, Peña E. 2016. Biaxial mechanical evaluation of absorbable and nonabsorbable synthetic surgical meshes used for hernia repair: physiological loads modify anisotropy response. Ann Biomed Eng. 44(7):2181–2188.

Van Craenenbroeck M, Mollaert M, De Laet L. 2019. The influence of test conditions and mathematical assumptions on biaxial material parameters of fabrics. Eng Struct. 200:1–23.

Deeken CR, Lake SP. 2017. Mechanical properties of the abdominal wall and biomaterials utilized for hernia repair. J Mech Behav Biomed Mater. 74:411–427. doi:10.1016/j.jmbbm.2017.05.008.

Est S, Roen M, Chi T, Simien A, Castile RM, Thompson DM, Blatnik JA, Deeken CR, Lake SP. 2017. Multi-directional mechanical analysis of synthetic scaffolds for hernia repair. J Mech Behav Biomed Mater. 71:43–53.

Fehervary H, Smoljkic M, Vander Sloten J, Famaey N. 2016. Planar biaxial testing of soft biological tissue using rakes: a critical analysis of protocol and fitting process. J Mech Behav Biomed Mater. 61:135–151.

Fehervary H, Vastmans J, Vander Sloten J, Famaey N. 2018. How important is sample alignment in planar biaxial testing of anisotropic soft biological tissues? A finite element study. J Mech Behav Biomed Mater. 88:201–216.

Gasser TC, Ogden RW, Holzapfel GA. 2006. Hyperelastic modelling of arterial layers with distributed collagen fibre orientations. J R Soc Interface. 3(6):15–35.

He W, Liu X, Wu S, Liao J, Cao G, Fan Y. 2020. A numerical method for guiding the design of surgical meshes with suitable mechanical properties for specific abdominal hernias. Comput Biol Med. 116:103531.

Hernández-Gascón B, Espés N, Peña E, Pascual G, Bellón JM, Calvo B. 2014. Computational framework to model and design surgical meshes for hernia repair. Comput Methods Biomech Biomed Engin. 17(10):1071–1085.

Hernández-Gascón B, Peña E, Grasa J, Pascual G, Bellón JM, Calvo B. 2013. Mechanical response of the herniated human abdomen to the placement of different prostheses. J Biomech Eng. 135:1–8.

Hernández-Gascón B, Peña E, Melero H, Pascual G, Doblaré M, Ginebra MP, Bellón JM, Calvo B. 2011. Mechanical behaviour of synthetic surgical meshes: finite element simulation of the herniated abdominal wall. Acta Biomater. 7(11):3905–3913.

Hoffmann H, Köckerling F, Adolf D, Mayer F, Weyhe D, Reinpold W, Fortelny R, Kirchhoff P. 2021. Analysis of 4,015 recurrent incisional hernia repairs from the Herniamed registry: risk factors and outcomes. Hernia [Internet]. 25(1):61–75.

Holzapfel GA. 2000. Nonlinear solid mechanics: a continuum approach for engineering. West Sussex: John Wiley & Sons, Inc.

Horbach AJ, Staat M. 2018. Optical strain measurement for the modeling of surgical meshes and their porosity. Curr Dir Biomed Eng. 4(1):181–184.

Kahan LG, Guertler C, Blatnik JA, Lake SP. 2017. Validation of single c-arm fluoroscopic technique for measuring in vivo abdominal wall deformation. J Biomech Eng. 139:84502.

Köhler G, Pallwein-Prettner L, Koch OO, Luketina RR, Lechner M, Emmanuel K. 2015. Magnetic resonance–visible meshes for laparoscopic ventral hernia repair. JSLS. 19(1):e2014.00175.

Li X, Kruger J, Jor J, Nielsen P, Nash M, Wong V, Dietz HP. 2014. Characterizing the ex vivo mechanical properties of synthetic polypropylene surgical mesh. J Mech Behav Biomed Mater. 37:48–55. doi:10.1016/j.jmbbm.2014.05.005.

Lubowiecka I. 2015a. Behaviour of orthotropic surgical implant in hernia repair due to the material orientation and abdomen surface deformation. Comput Methods Biomech Biomed Engin. 18(3):223–232.

Lubowiecka I. 2015b. Mathematical modelling of implant in an operated hernia for estimation of the repair persistence. Comput Methods Biomech Biomed Engin. 18(4):438–445.

Lubowiecka I, Tomaszewska A, Szepietowska K, Szymczak C, Śmietański M. 2020. In vivo performance of intraperitoneal onlay mesh after ventral hernia repair. Clin Biomech [Internet]. 78:105076.

Pierrat B, Al Abiad N, Le Ruyet A, Avril S. 2020. Multiscale mechanical characterization of knitted abdominal wall repair meshes. Comput Methods Biomech Biomed Engin. 23(sup1):S221–S222.

Röhrnbauer B, Kress G, Mazza E. 2014. A physically based structural model for a textile prosthetic mesh. Int J Solids Struct. 51(3-4):633–646.

Rynkevic R, Martins P, Fernandes A, Vange J, Gallego MR, Wach RA, Mes T, Bosman AW, Deprest J. 2019. In vitro simulation of in vivo degradation and cyclic loading of novel degradable electrospun meshes for prolapse repair. Polym Test [Internet]. 78:105957.

Saberski ER, Orenstein SB, Novitsky YW. 2011. Anisotropic evaluation of synthetic surgical meshes. Hernia. 15(1):47–52.

Sacks MS. 2000. Biaxial Mechanical Evaluation of Planar Biological Materials. J Elast. 61(1/3):199–246.

Szymczak C, Lubowiecka I, Szepietowska K, Tomaszewska A. 2017. Two-criteria optimisation problem for ventral hernia repair. Comput Methods Biomech Biomed Engin. 20(7):760–769.

Todros S, Pachera P, Pavan PG, Natali AN. 2018. Investigation of the mechanical behavior of polyester meshes for abdominal surgery: a preliminary study. J Med Biol Eng. 38(4):654–665.

Todros S, Pavan PG, Pachera P, Natali AN. 2017. Synthetic surgical meshes used in abdominal wall surgery: part II—biomechanical aspects. J Biomed Mater Res. 105(4):892–903.

Todros S, Pianigiani S, de Cesare N, Pavan PG, Natali AN. 2019. Marker tracking for local strain measurement in mechanical testing of biomedical materials. J Med Biol Eng. 39(5):764–772.

Tomaszewska A. 2016. Mechanical behaviour of knit synthetic mesh used in hernia surgery. Acta Bioeng Biomech. 18(1):77–86.

Tomaszewska A, Lubowiecka I, Szymczak C. 2019. Mechanics of mesh implanted into abdominal wall under repetitive load. Experimental and numerical study. J Biomed Mater Res B Appl Biomater. 107(5):1400–1409.

Velayudhan S, Martin D, Cooper-White J. 2009. Evaluation of dynamic creep properties of surgical mesh prostheses-uniaxial fatigue. J Biomed Mater Res. 91B(1):287–296.

Waldman SD, Lee JM, Barre Â. 2002. Boundary conditions during biaxial testing of planar connective tissues. Part 1: dynamic behavior. J Mater Sci Mater Med. 3:933–938.